ER reorganization and intracellular retention of CD58 are functionally independent properties of the human cytomegalovirus ER resident glycoprotein UL148

Christopher C. Nguyen,[a] Anthony J. Domma,[a] Hongbo Zhang,[a] and Jeremy P. Kamil[a, #]

Department of Microbiology and Immunology, LSU Health Sciences Center, Shreveport, Louisiana, USA[a]

Running Head: Charged-cluster-to-alanine mutagenesis of HCMV UL148

#Address correspondence to Jeremy P. Kamil, jkamil@lsuhsc.edu

1501 Kings Highway, Shreveport, Louisiana 71103

ABSTRACT

The human cytomegalovirus (HCMV) endoplasmic reticulum (ER)-resident glycoprotein UL148 is posited to play roles in immune evasion and regulation of viral cell tropism. UL148 prevents cell surface presentation of the immune cell costimulatory ligand CD58 while promoting maturation and virion incorporation of glycoprotein O, a receptor binding subunit for an envelope glycoprotein complex involved in entry. Meanwhile, UL148 activates the unfolded protein response (UPR) and causes large-scale reorganization of the ER. In an effort to determine whether the seemingly disparate effects of UL148 are related or discrete, we generated charged-cluster-to-alanine (CCTA) mutants of six charged clusters within the UL148 ectodomain, and compared them against wildtype UL148, in the context of recombinant viruses and in ectopic expression, assaying for effects on ER remodeling and CD58 surface presentation. Two mutants, targeting charged clusters spanning residues 79-83 (CC3) and 133-136 (CC4), respectively, retained the potential to impede CD58 presentation, and did so to an extent comparable to wildtype. Of the six mutants, only CC3 retained the capacity to reorganize the ER, showing a partial phenotype. Wildtype UL148 accumulates in a detergent-insoluble form during infection. However, all six CCTA mutants were fully soluble, which may imply a relationship between insolubility and organelle remodeling. Additionally, we found that the chimpanzee cytomegalovirus UL148 homolog suppresses CD58 presentation but fails to reorganize the ER, while the homolog from rhesus cytomegalovirus shows neither activity. Collectively, our findings illustrate varying degrees of functional divergence between homologous primate cytomegalovirus immunevasins and suggest that ER reorganization is unique to HCMV UL148.

45 **IMPORTANCE**

46 In myriad examples, viral gene products cause striking effects on cells, such as
47 activation of stress responses. It can be challenging to decipher how such effects
48 contribute to the biological roles of the proteins. The HCMV glycoprotein UL148 retains
49 CD58 within the ER, thereby preventing it from reaching the cell surface where it functions
50 to stimulate cell-mediated antiviral responses. Intriguingly, UL148 also triggers the
51 formation of large, ER-derived membranous structures, and activates the UPR, a set of
52 signaling pathways involved in adaptation to ER stress. We demonstrate that the
53 potential of UL148 to reorganize the ER and to retain CD58 are separable by mutagenesis
54 and possibly, by evolution, since chimpanzee cytomegalovirus UL148 retains CD58 but
55 does not remodel the ER. Our findings imply that ER reorganization contributes to other
56 roles of UL148, such as modulation of alternative viral glycoprotein complexes that govern
57 the virus' ability to infect different cell types.

58

59 **INTRODUCTION**

60 Cytomegaloviruses (CMVs), like other herpesviruses, encode a large and
61 multifarious array of gene products and regulatory RNAs that alter host cell functions to
62 support viral replication, spread, and lifelong persistence [reviewed in (1, 2)]. CMVs have
63 evolved a number of functions that dampen antiviral responses that otherwise produce
64 sterilizing immunity. Rodent and primate cytomegalovirus (CMV) species, such as mouse
65 cytomegalovirus (MCMV) and human cytomegalovirus (HCMV), express a large number
66 of proteins and microRNAs that interfere with antigen presentation and prevent activation
67 of cytotoxic T cells and NK cells [reviewed in (3-6)], (7). In HCMV, several viral gene
68 products involved in immune evasion, such as UL141 (8, 9), UL142 (10-12), and UL148
69 (13), are encoded within a region of the genome termed the 'UL*b'*,' which undergoes
70 extensive rearrangements and deletions during extensive serial passage in cultured cells
71 (14-16).

72 The HCMV glycoprotein UL148 impedes the activation of cytotoxic T-cell and NK
73 cell mediated responses by binding the co-stimulatory ligand CD58 and retaining it within
74 the endoplasmic reticulum (ER) (13). Intriguingly, UL148 also shows a strong capacity to
75 influence HCMV cell tropism, with *UL148*-null mutant viruses showing ~100-fold improved
76 replication in epithelial cells (17, 18). The evidence suggests that UL148 stabilizes
77 immature forms of glycoprotein O (gO) within the ER, thereby promoting the maturation
78 and incorporation into virions of the heterotrimeric glycoprotein H (gH)/ glycoprotein L
79 (gL)/ gO complex. gH/gL/gO (Trimer) and gH/gL/UL128-131 (Pentamer) are the two
80 alternative HCMV gH/gL complexes that endow the virus with the ability to utilize different
81 proteinaceous host cell surface factors as entry receptors [reviewed in (19)]. In particular,

82 gO, in the context of Trimer, is required for viral entry via the platelet-derived growth factor
83 receptor alpha (PDGFRα), which is well expressed in fibroblasts but poorly if at all in
84 epithelial cells (20-23). Infection of epithelial and endothelial cells, on the other hand,
85 appears to require direct interactions between the Pentamer and neuropilin-2 (Nrp2) (24),
86 together with roles for OR14I1 (25) and CD147 (26), addition to roles for the Trimer (27,
87 28). The striking replication advantage of *UL148*-null viruses in epithelial cells is
88 presumably explained by decreased expression of Trimer, which in turn is thought to favor
89 Pentamer-dependent interactions that are important for infection of epithelial cells.

90 Furthermore, UL148 is necessary and sufficient to activate the unfolded protein
91 response (UPR) (29), a canonical ER-stress adaptation pathway conserved among
92 eukaryotes. Although the mechanism for UPR activation remains unknown, UL148
93 appears to interact with the core ER-associated degradation (ERAD) factor SEL1L (18).
94 Hence, UL148 might be hypothesized to cause ER stress by impairing the ability of the
95 SEL1L/Hrd1 complex to dispose of misfolded proteins. Furthermore, UL148 drastically
96 reorganizes the ER, causing the accumulation of unusual electron-dense membranous
97 structures that appear to derive from distended rough-ER cisternae (30). These ER
98 structures are replete with factors involved in glycoprotein quality control such as SEL1L,
99 Hrd1, and EDEM1. We wondered whether the dramatic effects of UL148 on the ER might
100 be related to its potential to retain CD58. We therefore sought to develop experimental
101 approaches to interrogate whether these two UL148-dependent activities were separable
102 or interdependent.

103 In the absence of a three-dimensional structure, charged-cluster-to-alanine
104 (CCTA) mutagenesis provides a useful approach to identify functionally important

105 residues within a protein sequence. The underlying rationale is based on the assumption
106 that charged clusters of amino acids are more likely to be found on solvent exposed
107 surfaces in the context of the tertiary structure of a given polypeptide, and therefore
108 mutations affecting such residues are less likely to strongly influence overall protein
109 folding or stability (31-34). Additionally, charged clusters are often involved in biologically
110 relevant protein-protein interactions, as evidenced by the historical utility of CCTA
111 mutagenesis for identifying residues involved in ligand-receptor interactions (31, 35-38).
112 To define which UL148-associated activities may arise from shared versus distinct
113 molecular mechanisms, we combined CCTA mutagenesis with marker-less bacterial
114 artificial chromosome (BAC) recombination ("recombineering") methods (39, 40) to
115 generate HCMV genomes mutated for individual charged clusters within *UL148*. We also
116 constructed vectors for transient ectopic expression of UL148 CCTA mutants in non-
117 infected cells. Finally, we cloned UL148 homologs from other primate cytomegaloviruses,
118 including chimpanzee CMV (53% amino acid identity with UL148) and rhesus macaque
119 CMV (25% amino acid identity), so as to gain insight into potential evolutionary
120 relationships between the various activities of HCMV UL148.
121
122 **RESULTS**
123
124 **UL148 charged-cluster-to-alanine mutagenesis**
125 In order to identify charged residues within UL148 in an unbiased manner, we
126 utilized a simple scanning algorithm (window = 6 residues) to analyze the predicted
127 ectodomain of UL148. We designated any window containing at least 40% charged

128 amino acids (K, R, D, E) to be a charged cluster (**FIG 1A**). For practical purposes, we
129 opted to treat as a single cluster three clusters that were found in very close proximity to
130 each other (residues 220-231). In this manner, we were able to focus our mutagenesis
131 strategy on six charged clusters within the UL148 ectodomain (**FIG 1B**). We constructed
132 a series of expression plasmids encoding HA-tagged UL148 harboring CCTA mutations
133 at each of the clusters. For comparative purposes, we also cloned UL148 homologs from
134 two other primate CMVs—notably UL148 homologs are found only in primate CMVs. In
135 particular, we constructed plasmids encoding chimpanzee CMV UL148 (Ch148; 53%
136 identity) and rhesus CMV Rh159 (25% identity), each appended at its C-terminus to an
137 influenza virus hemagglutinin (HA) epitope tag.
138
139 **Expression of UL148 CCTA mutants and UL148 homologs.**
140 As a first step to confirm the expression of the UL148 CCTA mutants, and the
141 primate CMV homologs of UL148, we transfected HEK-293T (293T) cells with the
142 different expression plasmids. Robust levels of protein expression were observed for
143 both Rh159 and Ch148 (**FIG 2**). HCMV UL148 expressed to visibly lower levels than
144 Rh159 or Ch148 during transient overexpression in transfected cells. We interpret the
145 somewhat lower peak expression level of HCMV UL148 as likely being due to its
146 activation of the unfolded protein response (29). Nonetheless, each of the CCTA mutants
147 expressed at levels comparable to that of wildtype UL148, except perhaps CCTA mutant
148 #6, which affected the largest cluster (residues 220-231). Overall, each of the CCTA
149 constructs was readily detected following transient transfection of 293T cells (**FIG 2**).
150

151 **Disruption of four out of six charged clusters abolishes UL148-dependent**
152 **suppression of cell surface CD58**

153 Wang *et al*. (13) reported that HCMV UL148 is necessary and sufficient to
154 suppress surface presentation of CD58, a ligand for CD2 that co-stimulates T and NK cell
155 activation, such as in response to HCMV infection. Since CCTA mutagenesis has been
156 extensively used to define "interface" residues involved in protein-protein interactions, we
157 asked whether UL148 mutants ablated for specific charged clusters would show
158 differences in their ability to suppress CD58 surface presentation. Turning to a transient
159 expression system to ask this question, we electroporated UL148-CCTA constructs into
160 A549 lung adenocarcinoma cells, which basally express surface CD58 (see below). In
161 order to limit our analyses to cells that took up plasmid, we co-transfected a GFP
162 expression vector along with each UL148 construct. Gating for GFP positive cells, we
163 observed a ~40% decrease in CD58 median fluorescence intensity (MFI) in cells
164 transfected with wildtype UL148 (**FIG 3A**). A comparable decrease in surface CD58 was
165 detected in cells transfected with Ch148 expression vector but not with the vector
166 expressing the rhesus CMV UL148 homolog, Rh159. Importantly, four of our six CCTA
167 mutants failed to downregulate surface CD58. The remaining two CCTA constructs,
168 however, mutated at charged clusters #3 or #4, (**FIG 1B**), suppressed CD58 surface
169 presentation comparably to wildtype UL148.

170 We next sought to analyze the importance of the charged clusters in the context
171 of infection. We employed *en passant* mutagenesis (39, 40) to construct HCMV
172 recombinants harboring these CCTA mutations. Upon infection of fibroblasts with the
173 CCTA mutant viruses, we obtained results that largely recapitulate our findings from

174 electroporation of A549 cells with plasmid expression vectors (**FIG 3B**). The four different
175 charged clusters identified to be required for CD58 suppression in transient transfection
176 were likewise required to suppress CD58 surface presentation during HCMV infection.
177 Moreover, the two CCTA mutants competent for CD58 suppression in transfected A549
178 cells, CC3 and CC4, likewise appeared to suppress CD58 and did so indistinguishably
179 from parental wildtype virus. These results suggest that the two charged clusters at 79-
180 83 (CC3) and 133-136 (CC4) are dispensable for intracellular retention of CD58.
181 Additionally, our results indicate that the other four charged clusters are either directly
182 required to prevent surface presentation of CD58, or otherwise necessary for UL148 to
183 properly fold or function, since these mutant viruses phenocopy *UL148*-null virus
184 (148_{STOP}) in failing to downregulate CD58 surface levels.
185

186 **The propensity of UL148 to accumulate in a detergent-insoluble form is**
187 **dispensable for suppression of CD58 surface presentation.**

188 We recently observed that UL148 accumulates in a detergent-insoluble form
189 during infection (30). We therefore wished to examine whether any of the CCTA
190 mutations affected the solubility of UL148 during infection, since this could provide a clue
191 as to whether the UL148 insolubility is required for retention of CD58. We carried out
192 these experiments using fibroblasts infected with our series of recombinant HCMVs
193 expressing the six different CCTA mutants, so as to minimize the potential for artifacts
194 concerning solubility that might confound results obtained from transient overexpression
195 of plasmids. Each of the CCTA mutants failed to accumulate in the detergent-insoluble
196 fraction, while wildtype UL148, as expected appeared in both the soluble and insoluble

197 fractions (**FIG 4**). Nonetheless, cells infected with CCTA mutants affecting the clusters #3
198 (residues 79-83) and #4 (residues 133-136) showed defects in CD58 maturation matching
199 those seen with wildtype virus (**FIG 4**), which suggests that the potential for UL148 to
200 accumulate in a detergent-insoluble form is separable from its capacity to prevent CD58
201 maturation.
202
203 **Five out of six charged clusters are necessary for UL148-mediated ER remodeling**
204 UL148 activates the unfolded protein response (UPR), both during infection and
205 ectopic expression (29), and is also necessary and sufficient to drastically remodel the
206 ER (30). Hoping to identify charged clusters necessary for these striking effects, we again
207 turned to our panel of CCTA mutants. Results from confocal immunofluorescence
208 microscopy of infected cells stained for Hrd1 and UL148 (HA tag) at 72 h post-infection
209 (hpi) indicated that five of the six CCTA mutants matched the phenotype seen for *UL148*-
210 null virus (148_{STOP}) in failing to cause ER remodeling, as indicated by Hrd1 staining (**FIG**
211 **5**). The remaining mutant (CC3) exhibited a partial phenotype wherein UL148 puncta
212 formation could be detected in a minority of cells. Interestingly, the CC4 mutant
213 completely lost the ability to remodel the ER but nonetheless blocks maturation and
214 surface presentation of CD58 similarly if not equivalently to wildtype (**FIG 3-4**). Because
215 both CC3 and CC4 mutants block CD58 surface presentation while exhibiting,
216 respectively, either a significant decrease or a complete loss of ER remodeling, our
217 results suggest that these two activities involve distinct molecular mechanisms.
218
219 **The chimpanzee CMV UL148 homolog does not remodel the ER**

220 Lastly, we sought to determine whether the effects of UL148 on the ER and on
221 CD58 surface expression might be conserved by assaying HCMV UL148 against its
222 homologs from other primate CMVs. Rh159, the rhesus CMV homolog, shares 25%
223 amino acid identity with HCMV UL148 and has been shown to retain NKG2D receptor
224 activating ligands of the MIC- and ULBP families (7). Furthermore, Rh159 fails to activate
225 the UPR and does not appear to remodel ER membranes (29, 30). However, the
226 chimpanzee CMV homolog of UL148, Ch148, shares 53% amino acid identity with UL148,
227 and to the best of our knowledge has not been examined for its effects on CD58 or on
228 the ER. We cloned Ch148 fused at its predicted C-terminal tail to enhanced GFP (GFP)
229 in the context of an inducible expression vector to facilitate observation of Ch148
230 localization patterns within the cell. We previously constructed similar vectors encoding
231 Rh159 and UL148 fused to GFP (30). Upon induction of protein expression using 100
232 ng/mL doxycycline, we observed the formation of punctate structures for UL148-GFP but
233 diffuse, reticulate signal for Rh159-GFP, as expected (30). Interestingly, Ch148-GFP
234 exhibited a diffuse localization pattern more similar to that of Rh159 than UL148 (**FIG 6**).
235 Taken together with the results from our series of CCTA mutants, this result suggests that
236 ER remodeling and CD58 retention arise from distinct mechanisms.
237

238 **DISCUSSION**

239

240 **Evidence of distinct mechanisms for CD58 suppression and ER remodeling**

241 Upon discovering that UL148 reorganizes the ER (30), we wondered whether this
242 phenotype might play a role in ER-retention of CD58. We considered the possibility that
243 perhaps CD58 is so efficiently chaperoned to the cell surface that it somehow resists
244 being sequestered via simple high affinity interactions with an ER-resident protein. So
245 perhaps UL148 forms bizarre membranous structures to more potently obstruct its
246 presentation at the cell surface? Two findings from this study argue against this
247 possibility, and instead indicate that ER reorganization is dispensable for UL148-
248 mediated interference with CD58 surface presentation. Firstly, the CCTA mutant affecting
249 charged cluster #4 fails to remodel the ER but impedes CD58 surface presentation
250 comparably, if not indistinguishably, from wildtype UL148 (**FIG 3-5**). Secondly, the UL148
251 homolog from chimpanzee CMV (Ch148) is sufficient to suppress surface CD58
252 presentation but fails to induce the formation of punctate structures that we consistently
253 observe during expression of HCMV UL148, which indicate ER reorganization (30) (**FIG**
254 **3A, 6**). Although we cannot exclude the possibility that Ch148 suppresses CD58 surface
255 presentation by a mechanism distinct from that of HCMV UL148, we consider this to be
256 unlikely, considering the extensive sequence homology between Ch148 and HCMV
257 UL148 (>50% amino acid identity). A summary view of the observed activities for Ch148
258 and UL148 constructs is shown in **FIG 7**. Collectively, the data suggest that the properties
259 of UL148 that give rise to ER re-organization are distinct from those involved in
260 intracellular retention of CD58.

261

262 **Why does UL148 accumulate in a detergent-insoluble form, and what is the**
263 **relationship to ER reorganization?**

264 Fundamental to the biology of the ER is its system of mechanisms, such as N-
265 glycosylation and ER-resident chaperones, that function to prevent proteins from
266 aggregating or accumulating in an insoluble state (41, 42). Therefore, it seems unusual
267 that the wildtype form of an ER resident glycoprotein like UL148 would accumulate in a
268 detergent-insoluble form in the first place. Moreover, this feature of UL148 stands in stark
269 contrast with every other glycoprotein we have analyzed in infected cells, including gB
270 and CD58 (**FIG 4**), the RhCMV UL148 homolog Rh159 (30), as well as gH and gO (C.C.N.
271 and J.P.K., unpublished results). Surprisingly, all six of the CCTA mutants examined in
272 this study failed to accumulate in a detergent-insoluble form. Thus, a property readily
273 disrupted by CCTA mutagenesis is required for the protein to accumulate in an insoluble
274 form.

275 Notably, insoluble forms of many different proteins characteristically accumulate
276 during treatments that diminish proteasomal or lysosomal protein degradation pathways
277 (43-45). Conversely, protein aggregates are themselves thought to inhibit the ubiquitin
278 proteasome system (46). Intriguingly, UL148, exhibits a marked tendency toward
279 insolubility even in the absence of inhibitors affecting rates of protein degradation. We
280 hypothesize that the native conformer adopted by wildtype UL148 may resist ER
281 associated degradation (ERAD), and perhaps even generally inhibit ERAD. On the other
282 hand, other examples of proteins that form ER structures, such as the Z-allele of alpha-
283 1-antitrypsin (*SERPINA*) (47, 48), or the A103E mutant of the calcium channel subunit

284 ORAI1 (*CRAMC1*), exhibit a propensity to aggregate or polymerize within the ER, which
285 may make them resistant to ERAD. Given their improved solubility, each of the UL148
286 CCTA mutants, in contrast, might be predicted to show improved susceptibility to ERAD,
287 and may also indicate that these mutants no longer aggregate or polymerize.

288 Strikingly, five of the six CCTA mutants fully lost the ability to reorganize the ER,
289 while the one mutant that still showed ER organization exhibited a partial phenotype. It
290 is notable that in all cases, the loss of ER reorganization correlated with markedly
291 improved solubility. These observations collectively suggest that the propensity of UL148
292 to accumulate in an insoluble form may be mechanistically important for ER remodeling.
293

294 **Roles of ER remodeling cell tropism versus roles in immune evasion?**

295 Collectively, our results suggest that ER remodeling is indicative of, if not directly
296 involved, in a function unrelated to CD58 retention, since ER remodeling appears to be
297 dispensable for this function (**FIG 3-6**). Accordingly, one might hypothesize ER
298 reorganization to play roles in the cell tropism effects of UL148. The effects of UL148 on
299 HCMV cell tropism correlate with its potential to promote the expression of gH/gL/gO, a
300 heterotrimeric complex that endows virions with the ability to utilize PDGFRα as an entry
301 receptor (20, 21, 49, 50). We previously found that gO behaves as a constitutive ERAD
302 substrate and that UL148 stabilizes its expression (18). Given that the ER structures
303 induced by UL148 contain huge amounts of glycoprotein quality control proteins that
304 participate in ERAD (30), it seems plausible that UL148 may limit degradation of immature
305 gO by sequestering the ERAD machinery. Despite that a role for ER remodeling in

306 suppression of CD58 surface presentation seems unlikely, given our findings here, a role
307 in regulation of glycoprotein complexes involved in cell tropism remains to be disproven.
308

309 **Proper folding of UL148 harboring CCTA mutations**

310 In the absence of characterized monoclonal antibodies against UL148, we are
311 limited in our ability to conclusively demonstrate that the UL148 species carrying mutated
312 charged clusters fold properly in the ER. That said, our results offer some insight into the
313 overall stability of the proteins expressed from our plasmid constructs and recombinant
314 viruses. It is notable that all of six of the CCTA mutants we examined in this study show
315 improved solubility relative to wildtype UL148. Insolubility is often associated with
316 misfolding and aggregation. Therefore, the observation that wildtype UL148 is less
317 soluble that its CCTA mutants may suggest that insolubility is important for one or more
318 of its biological functions, but not for CD58 retention, as our results have identified two
319 CCTA mutants that retain CD58 without accumulating in an insoluble form. Even so,
320 caution compels us to avoid making strong conclusions from the other four CCTA mutants
321 that have so far only recapitulated *UL148*-null phenotypes with regard to ER remodeling
322 and CD58 retention. We are therefore focusing on mutants of charged clusters #3 (CC3)
323 and #4 (CC4) in our ongoing studies concerning UL148-mediated ER remodeling, since
324 CCTA mutants of these clusters can be presumed to fold properly, given that they remain
325 able to suppress CD58 maturation.
326

327 **Inferences into the UL148-CD58 interaction face**

328 Alanine scanning and CCTA mutagenesis approaches have proven useful to
329 define the specific amino acid residues underlying biologically relevant protein-protein
330 interactions. Despite that detailed empirical data on the tertiary structure of UL148 as-of-
331 yet remain unavailable, the results from our studies of UL148 CCTA mutants support a
332 number of inferences concerning the physical basis for its interaction with CD58. The two
333 charged clusters that do not appear to be important for CD58 retention, #3 and #4, are
334 found in a contiguous stretch of amino acids (residues 79-136) that lacks other charged
335 clusters. Assuming our other four CCTA mutants do not grossly compromise UL148
336 folding, residues from the N-terminal half (residues 47-62) and C-terminal half (residues
337 172-230) of the UL148 ectodomain may participate in an interaction face with CD58.
338 Likewise, our data suggest that the contiguous sequence containing clusters #3 and #4
339 represents a region within the 3D structure that does not participate in CD58 binding.
340

341 **Chimpanzee CMV provides a valuable model for comparative studies of HCMV**
342 **gene products in cell-based assays.**

343 Taken together, our findings highlight the various functionally divergent roles
344 among three different UL148 homologs in CMVs endemic to humans, rhesus
345 macaques, and chimpanzees. While all three proteins act as ER-resident
346 immunevasins, the rhesus CMV homolog lacks the potential to trigger the UPR (29, 30),
347 and apparently functions to evade NK cells by preventing MIC- and ULBP family
348 NKG2D ligands from reaching the cell surface (7). Chimpanzee and human CMV
349 UL148 target CD58 instead of NKG2D ligands [(13), **FIG 3**)], but only HCMV UL148 is
350 capable of remodeling the ER (**FIG 6**), a property that appears to depend on the

351 capacity of UL148 to activate the integrated stress response downstream of UPR
352 activation (30). Although chimpanzee CMV is more closely related to HCMV than
353 rhesus CMV (51), the use of chimpanzees as an animal model for human diseases is
354 prohibited, which likely has limited the interest of researchers in studying the virus. Our
355 study, however, highlights the utility of studying chimpanzee CMV gene products, even
356 in the context of cultured cells, to gain comparative insights into the functions of HCMV
357 genes. Chimpanzee CMV homologs may be of particular importance for helping us to
358 understand the functions of genes in regions of the virus such as the UL*b'*, which are
359 not well conserved, if at all, in rodent CMVs. Moreover, at least in the example of
360 UL148, the chimpanzee homolog appears to be more functionally aligned with HCMV
361 UL148 than the rhesus CMV homolog. Because genes within the UL*b'* play crucial
362 roles in latency, persistence, cell tropism, and immune evasion, elucidating their
363 functions will be of critical importance. A clear picture of which gene specific functions
364 are shared and divergent between the different primate CMVs may provide profound
365 insights into the unique biology of HCMV.

366 **MATERIALS AND METHODS**

367 **Cells.** Human telomerase (hTERT)-immortalized human foreskin fibroblasts (HFFT) were
368 described previously (18), and were cultured in Dulbecco's modified Eagle's medium
369 (DMEM; Corning Cat #10-013-CV) supplemented with 25 µg/mL gentamicin sulfate
370 (Invitrogen), 10 µg/mL ciprofloxacin HCl (Genhunter, Inc.) and 5% newborn calf serum
371 (NCS) (Sigma #N4637). Human embryonic kidney 293T (HEK-293T) cells were obtained
372 from Genhunter, Inc. (Nashville, TN), and cultured in DMEM supplemented as above
373 except with 10% fetal bovine serum (FBS) (MilliporeSigma Cat #F2442) instead of NCS.
374 A549 adenocarcinoma cells were obtained from ATCC (Cat # CCL-185) and grown in
375 Ham's F-12K medium (ThermoFisher, Cat # 21127022) supplemented with 10% FBS and
376 antibiotics, as above.

377

378 **Virus.** Virus was reconstituted by electroporation of purified bacterial artificial
379 chromosome (BAC) DNA into HFFT and amplified until 100% cytopathic effect (CPE) was
380 observed, as previously described (17, 18, 52). Cell-free virus in the medium was
381 combined with cell-associated virus, which was released by Dounce-homogenization of
382 the cells. Virus preparation was clarified of cellular debris by centrifugation (4000 × *g*, 10
383 min), followed by pelleting of virus by ultracentrifugation (85,000 × *g*, 1 h, 4°C) through a
384 20% sorbitol cushion. The supernatant was removed, and the viral pellet was
385 resuspended in DMEM supplemented with 20% NCS and stored at -80°C.

386

387 **Virus titration.** Infectivity of virus stocks was determined according to the tissue culture
388 infectious dose 50% ($TCID_{50}$) method. In brief, stocks were serially diluted, and diluted

389 virus was used to infect eight wells per dilution in a 96-well plate seeded one day prior
390 with 3 × 10^4 HFFT per well. Infection was allowed to proceed for 9 days before IE1
391 staining as follows. Cells were washed (3 × 200 µL PBS per well) and fixed in ice-cold
392 methanol (200 µL/well, 15 min at -20°C). Cells were washed (3 × 200 µL PBS per well)
393 and stained with 1:200 mouse anti-IE1 primary antibody (supernatant from IE1 mAb 1B12
394 hybridoma cells, a generous gift of Thomas Shenk, Princeton University) for 1 h at 37°C.
395 Cells were washed (3 × 200 µL PBS per well) and stained with 1:1000 goat anti-mouse
396 Alexa Fluor 488 secondary antibody (ThermoFisher, Cat # A-11001) for 1 h at 37°C. The
397 cells were washed (1 × 200 µL PBS per well) and incubated for 1 min with 1 µg/mL
398 Hoechst 33342 (ThermoFisher, Cat# H3570) to counterstain nuclei. Virus plaques were
399 visualized under LED epifluorescence using a Nikon Eclipse Ts2R microscope (Nikon
400 Instruments, Inc, Melville, NY), and each well was scored positive or negative if at least
401 one virus plaque was visible. Infectivity in $TCID_{50}$ units was calculated according to the
402 Spearman-Kärber method, as described previously (18).
403
404 **Plotting of charged clusters within the UL148 ectodomain.** The percentage (charged
405 residues/total residues) in each 6-residue window was plotted using a Python script and
406 visualized using Prism 8 software (GraphPad, Inc., San Diego, CA). Eight local maxima
407 were identified at amino acid positions 47-52, 59-62, 79-83, 133-136, 172-177, 222-225,
408 223-227, 225-230. Because of their close proximity to each other, the final three clusters
409 were regarded as a single charged cluster for the purposes of constructing mutants.
410

411 **Expression vectors encoding HA-tagged UL148 harboring charged-cluster-to-**
412 **alanine mutations.** pcDNA3.1+ UL148HA was generated as follows. A PCR product
413 encoding the HA-tagged *UL148* open reading frame was amplified from template plasmid
414 pEF1α UL148HA (18) using primers UL148_reclone_FWD and UL148_reclone_REV.
415 PCR product was digested with BamHI/EcoRI and ligated into BamHI/EcoRI-digested
416 pcDNA3.1+ (Invitrogen) to yield pcDNA3.1+ UL148HA, which was sequence-confirmed
417 using primers CMV_FWD and BGH_REV.
418 HA-tagged UL148 was subcloned from pcDNA3.1+ into pSP72 as follows.
419 pcDNA3.1+ UL148HA was digested with BamHI/EcoRI. The ~1kb fragment was agarose-
420 purified and ligated into BamHI/EcoRI-digested pSP72. Overlapping primers (Table 1)
421 were used to amplify the pSP72 UL148HA template and introduce charged-cluster-to-
422 alanine (CCTA) mutations into the *UL148* open reading frame (ORF). PCR products were
423 digested with DpnI for 1 h at 37°C to remove template plasmid before transformation and
424 isolation of carbenicillin-resistant clones, which were confirmed by enzyme digestion and
425 sequencing using primers SP6_FWD and T7_seq_FWD. These mutated *UL148*
426 sequences were then transferred back to pcDNA3.1+ by BamHI/EcoRI digestion and
427 ligation as above.
428
429 **Expression vectors encoding HA-tagged chimpanzee CMV UL148 and rhesus CMV**
430 **Rh159.** pcDNA3.1+ Rh159HA was described previously (29). pcDNA3.1+ encoding HA-
431 tagged chimpanzee CMV UL148 was constructed by Gibson assembly of gBlock
432 ChCMV_UL148_FRAG with BamHI/EcoRI-digested pcDNA3.1+ (Invitrogen) and
433 sequence-confirmed using primers CMV_FWD and BGH_REV. The coding sequence

434 for chimpanzee CMV UL148 (Panine herpesvirus 2 strain Heberling, Genbank/ NCBI
435 Reference Sequence: NC_003521.1) was codon-optimized by Integrated DNA
436 Technologies (Coralville, IA), based on *Homo sapiens* codon usage, to facilitate synthesis
437 as a synthetic dsDNA gBlock.
438
439 **Inducible expression vectors encoding EGFP fused to UL148 homologs of human,**
440 **chimpanzee, and rhesus CMV.** Inducible lentiviral vectors pOUPc-UL148-eGFP and
441 pOUPc-Rh159-eGFP were described previously (30). pOUPc encoding chimpanzee
442 CMV UL148 fused to eGFP was constructed as follows. Fragment (i) was amplified using
443 primers Fwd_Ch148_OUPgibs and Rev_Ch148_GFPgibs with pcDNA3.1+ ChCMV
444 UL148HA as a template. Fragment (ii) was amplified using primers Fwd_GFP_Ch148gibs
445 and Rev_GFP_allUL148 using pOUPc-UL148-eGFP as a template. Fragments (i) and (ii)
446 were combined with AgeI/MluI-digested pOUPc in Gibson assembly to yield pOUPc-
447 Ch148-eGFP, which was sequence-confirmed using primers CMVcrsnull_Fw, Ubc_Rv,
448 and Ch148_3pr_Fw.
449
450 **Construction of recombinant viruses.** Synthetic double-stranded DNA (gBlocks) and
451 oligonucleotides were purchased from Integrated DNA Technologies; sequences are
452 provided in **Table 1**. All mutagenesis procedures was performed in the context of the
453 infectious BAC clone of HCMV strain TB40/E, TB40-BAC4 (53), as previously described
454 (17, 18, 29, 52, 54). Briefly, two-step Red "*en passant*" recombination (39, 40) was used
455 in conjunction with GS1783 *E. coli* (a gift of Greg Smith, Northwestern University)
456 harboring derivatives of TB40-BAC4. Recombinant BACs were confirmed by Sanger-

457 sequencing (Genewiz, Inc., South Plainfield, NJ) of modified loci (not shown), and by
458 BamHI and EcoRI restriction enzyme digestion analysis to exclude spurious
459 rearrangements (not shown).
460
461 **Recombinant HCMVs encoding HA-tagged UL148 and S-tagged glycoprotein O.**
462 Recombinant HCMV, strain TB40/E, encoding S-tagged glycoprotein O and HA-tagged
463 UL148 (TB_148^{HA}_gO^{S}) was constructed by insertion of a S-tag at the C-terminus of the
464 *UL74* open reading frame, essentially as in (18), but in the context of recombinant
465 TB_148^{HA} (17). Briefly, plasmid pSP72-*UL74-S-ISceKan* (18) was digested with EcoRV,
466 and the 1.4 kb band was agarose-purified and recombined into TB_148^{HA}. Kan-resistant
467 integrate colonies were isolated and resolved of the Kan cassette by L(+)-arabinose
468 induction of the homing endonuclease ISce-I and the bacteriophage lambda Red
469 recombinase system. Kan-sensitive clones were sequence-confirmed using primers
470 TB_UL74_Cterm_seq_FWD and TB_UL74_Cterm_seq_REV.
471
472 **Recombinant HCMVs encoding CCTA mutations within *UL148*.** CCTA mutations
473 were introduced into TB_148^{HA}_gO^{S} as follows. A PCR product containing an I-SceI
474 restriction site upstream of a kanamycin (Kan) resistance cassette and 40-bp flanks
475 homologous to the sequence surrounding each *UL148* charged cluster was amplified
476 using primers indicated in Table 1 and TB_148_ISceKan BAC DNA (17) as the template.
477 The gel-purified PCR product was electroporated into GS1783 *E. coli* carrying an
478 infectious BAC clone of TB_148^{HA}_gO^{S}. After isolating Kan-resistant colonies, the Kan
479 expression cassette was “scarlessly” resolved by inducing expression of the I-SceI

480 homing endonuclease and Red recombinase. The final Kan-sensitive
481 TB_148^{HA}_CCTA_gO^{S} recombinants were sequence-confirmed using primers
482 TB_Rh159HA_seq_FWD and TB_Rh159HA_seq_REV.
483
484 **Antibodies.** Antibody dilutions for Western blot included 1:1000 rabbit anti-HA (Bethyl),
485 1:250 mouse anti-CD58 (Invitrogen #MA5800). For flow cytometry, APC-conjugated
486 mouse anti-CD58 antibody (Invitrogen #17-0578) and isotype control (Invitrogen #17-
487 4714) were used at 1:40 dilution. For confocal microscopy, chicken anti-HA (Bethyl) and
488 rabbit anti-Hrd1 (Cell Signaling Technology) were used at a dilution of 1:200. Goat anti-
489 chicken Alexa Fluor 647 (Invitrogen) and goat anti-rabbit Alexa Fluor 488 (Invitrogen)
490 secondary antibodies were used at 1:1000.
491

492 **Surface CD58 quantification by flow cytometry.** For experiments in transfected cells,
493 1.2×10^6 A549 cells were electroporated using a Lonza Nucleofector™ 2B device
494 (program X-001) with 1.5 µg pcDNA3.1+ encoding the indicated protein plus 1 µg
495 pmaxGFP™ (Amaxa) in Ingenio nucleofection buffer (Mirus, Inc., cat # MIR 50114) .
496 Electroporated cells were then seeded to a 6-well cluster dish and incubated at 37°C
497 until 72 h post-transfection. For experiments in infected fibroblasts, 1.0×10^5 cells were
498 seeded into 6-well cluster dishes and infected at an MOI of 2 $TCID_{50}$/cell with
499 TB_148$_{HA}$_gO^{S} or the derived CCTA mutant viruses. The following day, the viral inocula
500 were removed, and media were replenished with fresh 5% newborn calf serum
501 (NCS)/DMEM. The cells were incubated at 37˚C until 72 h post-infection. Infected cells
502 were formalin-fixed before the CD58-staining step below.

503 At time of analysis, cells were detached using a 1:10 dilution of TrypLE^{TM}
504 Express (Gibco #12605) solution. Cells were pelleted (5 min, 300 × *g*) and resuspended
505 in FACS buffer [5% NCS in PBS]. Cells were incubated with APC-conjugated anti-CD58
506 antibody or isotype control for 1 h at 4°C with rotation, then washed three times with
507 FACS buffer and analyzed by flow cytometry. In transfection experiments, cells were
508 first gated on GFP to remove any non-transfected cells from the analysis. Median APC
509 fluorescence values were determined for each condition, and all values were
510 normalized to the median APC signal of GFP+ cells transfected with empty pcDNA3.1+.
511 Graphs were generated in Prism 8 for Mac Os (GraphPad Software, Inc. San Diego,
512 CA).

513 **Analysis of protein solubility.** 2 × 10^5 fibroblasts (HFFT) were infected at an MOI of 1
514 $TCID_{50}$ per cell with TB_148^{HA}_gO^{S} or the derived CCTA mutants. The following day,
515 cells were washed once with PBS and replenished with fresh 5% NCS/DMEM. At 72 h
516 post-infection, cells were prepared for Western blot analysis of detergent-soluble and -
517 insoluble material as previously described (30). Briefly, cells were washed with PBS and
518 lysed by direct addition of RIPA buffer [25 mM 4-(2-hydroxyethyl)-1-
519 piperazineethanesulfonic acid (HEPES) pH 7.5, 400 mM NaCl, 0.1% sodium dodecyl
520 sulfate (SDS), 0.5% sodium deoxycholate, 1% NP-40], supplemented with 1× protease
521 inhibitor cocktail (ApexBio, Inc., Houston, TX, Cat #K1007) and rotated for 1 h at 4˚C.
522 Lysates were centrifuged (21,000 × *g*, 35 min) to separate soluble and insoluble
523 material. The supernatant containing soluble material was transferred to a new tube,
524 and Laemmli buffer was added to 1× final [50 mM Tris (pH 6.8), 2% SDS, 10% glycerol,
525 0.02% bromophenol blue]. Pellet containing insoluble material was lysed in 1× Laemmli

526 buffer. Samples were reduced by addition of beta-mercaptoethanol (5% final, v/v) and
527 boiled at 90˚C for 10 min. Samples were resolved by SDS-PAGE (12% polyacrylamide
528 gel) and transferred to nitrocellulose membrane. Membranes were blotted with indicated
529 antibodies and visualized by Odysey CLx scanner (Li-Cor, Inc., Lincoln, NE).

530

531 **Plasmid transfection.** For Western blot studies, 1 × 10^6 HEK-293T (293T) cells were
532 reverse-transfected with 2.5 µg pcDNA3.1+ encoding the indicated proteins, as follows.
533 TransIT-293 transfection reagent (Mirus Inc., Madison, WI, Cat #2700) was mixed with
534 plasmid DNA in Opti-MEM (ThermoFisher) according to the manufacturer's instructions.
535 After 25 min incubation at room temperature, the transfection reagent-DNA complexes
536 were added to 2 mL 5% FBS/DMEM containing 1 × 10^6 HEK-293T cells in suspension.
537 Cells and transfection reagent-DNA complexes were gently mixed and seeded to a 6-
538 well plate.

539 For immunofluorescence imaging, 7 × 10^4 293T cells were reverse-transfected
540 with 1 µg doxycycline-inducible pOUPc plasmid (29, 30) encoding the indicated protein
541 as follows. Plasmid DNA was combined with 7.5 µL of 1 mg/mL branched
542 polyethylenimine (PEI; Sigma #408727) in 160 µL of Opti-MEM and gently mixed. DNA-
543 PEI complexes were allowed to form at room temperature for 20 min. 1 mL of 5%
544 FBS/DMEM containing 7 × 10^4 293T cells was then added to the DNA-PEI solution and
545 mixed gently before seeding to a 96-well plate. After cells had attached to the well (1 h
546 post-transfection), doxycycline hyclate stock was added directly to each well to a final

547 concentration of 100 ng/mL. Cells were incubated at 37°C for 48 h before imaging for
548 GFP signal on a Nikon Eclipse Ts2R microscope (Nikon Instruments, Inc, Melville, NY).

549 **Confocal microscopy.** 7 × 10^5 fibroblasts (HFFT) were seeded on 12 mm round
550 coverslips (Azer Scientific, #200121) in a 24-well plate. The following day, cells were
551 infected at an MOI of 1 $TCID_{50}$ per cell with TB_148^{HA}_gO^{S} or the indicated
552 recombinants. At 72 h post-infection, cells were processed for confocal microscopy
553 essentially as in (30). Briefly, cells were washed once with 1 mL PBS, fixed in 4% (w/v)
554 paraformaldehyde/PBS for 20 min at room temperature, and permeabilized for 3 min by
555 0.1% TritonX-100. Coverslips were incubated in 5% (v/v) normal goat serum for 30 min
556 at room temperature. After washing three times with 1 mL PBS, coverslips were
557 incubated with 1% Human Fc Block (BD Biosciences, Cat # 564219) for 30 min at room
558 temperature. Coverslips were incubated with primary antibody for 1 h in a humid 37°C
559 incubator, washed three times in 1 mL PBS and then incubated in the presence of
560 secondary antibody (1 h, 37°C humid incubator), followed by three washes in PBS, as
561 above. Finally, coverslips were mounted onto glass slides in mounting medium [0.01 M
562 Tris (pH 8.8), 90% glycerol, 0.5% N-propyl gallate] and sealed with nail polish. Cells
563 were imaged on a Leica TCS SP5 confocal microscope using a Leica 63× oil immersion
564 objective lens.

565 **ACKNOWLEDGMENTS**

566 This project was supported by NIH Grants R01-AI116851 (to J.P.K) and P30-
567 GM110703. Its contents are solely the responsibility of the authors and do not
568 necessarily represent the official views of the funding agencies. C.C.N. was supported
569 by a Malcolm Feist Predoctoral Fellowship from the Center of Cardiovascular Diseases

570 and Sciences at LSU Health Sciences Center, Shreveport. Author contributions are as
571 follows: C.C.N. conceived of the study, designed research, constructed new
572 recombinant HCMVs and plasmid constructs, carried out most experiments, and
573 contributed to writing the manuscript. A.J.D. performed and contributed to the design of
574 the flow cytometry experiments with infected cells. J.P.K. designed research,
575 interpreted data, obtained funding, and contributed to writing the manuscript. H.Z.
576 assisted with confocal microscopy and constructed the recombinant virus
577 TB_148^{HA}_gO^{S}.

578 **REFERENCES**

579 1. Jackson SE, Mason GM, Wills MR. 2011. Human cytomegalovirus immunity and
580 immune evasion. Virus Res 157:151-60.
581 2. Mocarski ES, Shenk T, Griffiths PD, Pass RF. 2013. Cytomegaloviruses, p 1960-2014.
582 *In* Knipe DM, Howley PM (ed), Fields' Virology, 6th ed, vol 2. Wolters Kluwer
583 Health/Lippincott Williams & Wilkins, Philadelphia.
584 3. Goodier MR, Jonjic S, Riley EM, Juranic Lisnic V. 2018. CMV and natural killer cells:
585 shaping the response to vaccination. Eur J Immunol 48:50-65.
586 4. Lemmermann NA, Bohm V, Holtappels R, Reddehase MJ. 2011. In vivo impact of
587 cytomegalovirus evasion of CD8 T-cell immunity: facts and thoughts based on
588 murine models. Virus Res 157:161-74.
589 5. Wilkinson GW, Tomasec P, Stanton RJ, Armstrong M, Prod'homme V, Aicheler R,
590 McSharry BP, Rickards CR, Cochrane D, Llewellyn-Lacey S, Wang EC, Griffin CA,
591 Davison AJ. 2008. Modulation of natural killer cells by human cytomegalovirus. J Clin
592 Virol 41:206-12.
593 6. Goldberger T, Mandelboim O. 2014. The use of microRNA by human viruses: lessons
594 from NK cells and HCMV infection. Semin Immunopathol 36:659-74.
595 7. Sturgill ER, Malouli D, Hansen SG, Burwitz BJ, Seo S, Schneider CL, Womack JL,
596 Verweij MC, Ventura AB, Bhusari A, Jeffries KM, Legasse AW, Axthelm MK, Hudson
597 AW, Sacha JB, Picker LJ, Fruh K. 2016. Natural Killer Cell Evasion Is Essential for
598 Infection by Rhesus Cytomegalovirus. PLoS Pathog 12:e1005868.
599 8. Prod'homme V, Sugrue DM, Stanton RJ, Nomoto A, Davies J, Rickards CR, Cochrane
600 D, Moore M, Wilkinson GW, Tomasec P. 2010. Human cytomegalovirus UL141
601 promotes efficient downregulation of the natural killer cell activating ligand CD112.
602 J Gen Virol 91:2034-9.
603 9. Smith W, Tomasec P, Aicheler R, Loewendorf A, Nemcovicova I, Wang EC, Stanton RJ,
604 Macauley M, Norris P, Willen L, Ruckova E, Nomoto A, Schneider P, Hahn G, Zajonc
605 DM, Ware CF, Wilkinson GW, Benedict CA. 2013. Human cytomegalovirus
606 glycoprotein UL141 targets the TRAIL death receptors to thwart host innate
607 antiviral defenses. Cell Host Microbe 13:324-35.
608 10. Ashiru O, Bennett NJ, Boyle LH, Thomas M, Trowsdale J, Wills MR. 2009. NKG2D
609 ligand MICA is retained in the cis-Golgi apparatus by human cytomegalovirus
610 protein UL142. J Virol 83:12345-54.
611 11. Bennett NJ, Ashiru O, Morgan FJ, Pang Y, Okecha G, Eagle RA, Trowsdale J, Sissons JG,
612 Wills MR. 2010. Intracellular sequestration of the NKG2D ligand ULBP3 by human
613 cytomegalovirus. J Immunol 185:1093-102.
614 12. Wills MR, Ashiru O, Reeves MB, Okecha G, Trowsdale J, Tomasec P, Wilkinson GW,
615 Sinclair J, Sissons JG. 2005. Human cytomegalovirus encodes an MHC class I-like
616 molecule (UL142) that functions to inhibit NK cell lysis. J Immunol 175:7457-65.
617 13. Wang ECY, Pjechova M, Nightingale K, Vlahava VM, Patel M, Ruckova E, Forbes SK,
618 Nobre L, Antrobus R, Roberts D, Fielding CA, Seirafian S, Davies J, Murrell I, Lau B,
619 Wilkie GS, Suarez NM, Stanton RJ, Vojtesek B, Davison A, Lehner PJ, Weekes MP,
620 Wilkinson GWG, Tomasec P. 2018. Suppression of costimulation by human
621 cytomegalovirus promotes evasion of cellular immune defenses. Proc Natl Acad Sci
622 U S A 115:4998-5003.

623 14. Cha TA, Tom E, Kemble GW, Duke GM, Mocarski ES, Spaete RR. 1996. Human
624 cytomegalovirus clinical isolates carry at least 19 genes not found in laboratory
625 strains. J Virol 70:78-83.
626 15. Dargan DJ, Douglas E, Cunningham C, Jamieson F, Stanton RJ, Baluchova K, McSharry
627 BP, Tomasec P, Emery VC, Percivalle E, Sarasini A, Gerna G, Wilkinson GW, Davison
628 AJ. 2010. Sequential mutations associated with adaptation of human
629 cytomegalovirus to growth in cell culture. J Gen Virol 91:1535-46.
630 16. Murrell I, Wilkie GS, Davison AJ, Statkute E, Fielding CA, Tomasec P, Wilkinson GW,
631 Stanton RJ. 2016. Genetic Stability of Bacterial Artificial Chromosome-Derived
632 Human Cytomegalovirus during Culture In Vitro. J Virol 90:3929-43.
633 17. Li G, Nguyen CC, Ryckman BJ, Britt WJ, Kamil JP. 2015. A viral regulator of
634 glycoprotein complexes contributes to human cytomegalovirus cell tropism. Proc
635 Natl Acad Sci U S A 112:4471-6.
636 18. Nguyen CC, Siddiquey MNA, Zhang H, Li G, Kamil JP. 2018. Human Cytomegalovirus
637 Tropism Modulator UL148 Interacts with SEL1L, a Cellular Factor That Governs
638 Endoplasmic Reticulum-Associated Degradation of the Viral Envelope Glycoprotein
639 gO. J Virol 92:e00688-18.
640 19. Nguyen CC, Kamil JP. 2018. Pathogen at the Gates: Human Cytomegalovirus Entry
641 and Cell Tropism. Viruses 10.
642 20. Wu K, Oberstein A, Wang W, Shenk T. 2018. Role of PDGF receptor-alpha during
643 human cytomegalovirus entry into fibroblasts. Proc Natl Acad Sci U S A
644 doi:10.1073/pnas.1806305115.
645 21. Wu Y, Prager A, Boos S, Resch M, Brizic I, Mach M, Wildner S, Scrivano L, Adler B.
646 2017. Human cytomegalovirus glycoprotein complex gH/gL/gO uses PDGFR-alpha
647 as a key for entry. PLoS Pathog 13:e1006281.
648 22. Vanarsdall AL, Wisner TW, Lei H, Kazlauskas A, Johnson DC. 2012. PDGF receptor-
649 alpha does not promote HCMV entry into epithelial and endothelial cells but
650 increased quantities stimulate entry by an abnormal pathway. PLoS Pathog
651 8:e1002905.
652 23. Liu J, Jardetzky TS, Chin AL, Johnson DC, Vanarsdall AL. 2018. The human
653 cytomegalovirus trimer and pentamer promote sequential steps in entry into
654 epithelial and endothelial cells at cell surfaces and endosomes. J Virol
655 doi:10.1128/JVI.01336-18.
656 24. Martinez-Martin N, Marcandalli J, Huang CS, Arthur CP, Perotti M, Foglierini M, Ho H,
657 Dosey AM, Shriver S, Payandeh J, Leitner A, Lanzavecchia A, Perez L, Ciferri C. 2018.
658 An Unbiased Screen for Human Cytomegalovirus Identifies Neuropilin-2 as a Central
659 Viral Receptor. Cell 174:1158-1171 e19.
660 25. E X, Meraner P, Lu P, Perreira JM, Aker AM, McDougall WM, Zhuge R, Chan GC,
661 Gerstein RM, Caposio P, Yurochko AD, Brass AL, Kowalik TF. 2019. OR14I1 is a
662 receptor for the human cytomegalovirus pentameric complex and defines viral
663 epithelial cell tropism. Proc Natl Acad Sci U S A 116:7043-7052.
664 26. Vanarsdall AL, Pritchard SR, Wisner TW, Liu J, Jardetzky TS, Johnson DC. 2018.
665 CD147 Promotes Entry of Pentamer-Expressing Human Cytomegalovirus into
666 Epithelial and Endothelial Cells. MBio 9:e00781-18.
667 27. Wille PT, Knoche AJ, Nelson JA, Jarvis MA, Johnson DC. 2010. A human
668 cytomegalovirus gO-null mutant fails to incorporate gH/gL into the virion envelope

669 and is unable to enter fibroblasts and epithelial and endothelial cells. J Virol
670 84:2585-96.
671 28. Jiang XJ, Adler B, Sampaio KL, Digel M, Jahn G, Ettischer N, Stierhof YD, Scrivano L,
672 Koszinowski U, Mach M, Sinzger C. 2008. UL74 of human cytomegalovirus
673 contributes to virus release by promoting secondary envelopment of virions. J Virol
674 82:2802-12.
675 29. Siddiquey MNA, Zhang H, Nguyen CC, Domma AJ, Kamil JP. 2018. The Human
676 Cytomegalovirus Endoplasmic Reticulum-Resident Glycoprotein UL148 Activates
677 the Unfolded Protein Response. J Virol 92:e00896-18.
678 30. Zhang H, Read C, Nguyen CC, Siddiquey MNA, Shang C, Hall CM, von Einem J, Kamil
679 JP. 2019. A cytomegalovirus immunevasin triggers integrated stress response-
680 dependent reorganization of the endoplasmic reticulum. bioRxiv
681 doi:10.1101/641068:641068.
682 31. Cunningham BC, Wells JA. 1989. High-resolution epitope mapping of hGH-receptor
683 interactions by alanine-scanning mutagenesis. Science 244:1081-5.
684 32. Dao-pin S, Anderson DE, Baase WA, Dahlquist FW, Matthews BW. 1991. Structural
685 and thermodynamic consequences of burying a charged residue within the
686 hydrophobic core of T4 lysozyme. Biochemistry 30:11521-9.
687 33. Wertman KF, Drubin DG, Botstein D. 1992. Systematic mutational analysis of the
688 yeast ACT1 gene. Genetics 132:337-50.
689 34. Chothia C. 1976. The nature of the accessible and buried surfaces in proteins. J Mol
690 Biol 105:1-12.
691 35. Aroeti B, Kosen PA, Kuntz ID, Cohen FE, Mostov KE. 1993. Mutational and secondary
692 structural analysis of the basolateral sorting signal of the polymeric
693 immunoglobulin receptor. J Cell Biol 123:1149-60.
694 36. Graber P, Proudfoot AE, Talabot F, Bernard A, McKinnon M, Banks M, Fattah D,
695 Solari R, Peitsch MC, Wells TN. 1995. Identification of key charged residues of
696 human interleukin-5 in receptor binding and cellular activation. J Biol Chem
697 270:15762-9.
698 37. Banks M, Graber P, Proudfoot AE, Arod CY, Allet B, Bernard AR, Sebille E, McKinnon
699 M, Wells TN, Solari R. 1995. Soluble interleukin-5 receptor alpha-chain binding
700 assays: use for screening and analysis of interleukin-5 mutants. Anal Biochem
701 230:321-8.
702 38. Hebert CA, Vitangcol RV, Baker JB. 1991. Scanning mutagenesis of interleukin-8
703 identifies a cluster of residues required for receptor binding. J Biol Chem
704 266:18989-94.
705 39. Tischer BK, Smith GA, Osterrieder N. 2010. En passant mutagenesis: a two step
706 markerless red recombination system. Methods Mol Biol 634:421-30.
707 40. Tischer BK, von Einem J, Kaufer B, Osterrieder N. 2006. Two-step red-mediated
708 recombination for versatile high-efficiency markerless DNA manipulation in
709 Escherichia coli. Biotechniques 40:191-7.
710 41. Nishikawa SI, Fewell SW, Kato Y, Brodsky JL, Endo T. 2001. Molecular chaperones in
711 the yeast endoplasmic reticulum maintain the solubility of proteins for
712 retrotranslocation and degradation. J Cell Biol 153:1061-70.

713 42. Brodsky JL, Skach WR. 2011. Protein folding and quality control in the endoplasmic
714 reticulum: Recent lessons from yeast and mammalian cell systems. Curr Opin Cell
715 Biol 23:464-75.
716 43. Kaganovich D, Kopito R, Frydman J. 2008. Misfolded proteins partition between two
717 distinct quality control compartments. Nature 454:1088-95.
718 44. Codony-Servat J, Tapia MA, Bosch M, Oliva C, Domingo-Domenech J, Mellado B, Rolfe
719 M, Ross JS, Gascon P, Rovira A, Albanell J. 2006. Differential cellular and molecular
720 effects of bortezomib, a proteasome inhibitor, in human breast cancer cells.
721 Molecular Cancer Therapeutics 5:665-675.
722 45. Latonen L, Moore HM, Bai B, Jaamaa S, Laiho M. 2011. Proteasome inhibitors induce
723 nucleolar aggregation of proteasome target proteins and polyadenylated RNA by
724 altering ubiquitin availability. Oncogene 30:790-805.
725 46. Bence NF, Sampat RM, Kopito RR. 2001. Impairment of the ubiquitin-proteasome
726 system by protein aggregation. Science 292:1552-5.
727 47. Cox DW, Billingsley GD, Callahan JW. 1986. Aggregation of plasma Z type alpha 1-
728 antitrypsin suggests basic defect for the deficiency. FEBS Lett 205:255-60.
729 48. Lomas DA, Evans DL, Finch JT, Carrell RW. 1992. The mechanism of Z alpha 1-
730 antitrypsin accumulation in the liver. Nature 357:605-7.
731 49. Kabanova A, Marcandalli J, Zhou T, Bianchi S, Baxa U, Tsybovsky Y, Lilleri D, Silacci-
732 Fregni C, Foglierini M, Fernandez-Rodriguez BM, Druz A, Zhang B, Geiger R, Pagani
733 M, Sallusto F, Kwong PD, Corti D, Lanzavecchia A, Perez L. 2016. Platelet-derived
734 growth factor-alpha receptor is the cellular receptor for human cytomegalovirus
735 gHgLgO trimer. Nat Microbiol 1:16082.
736 50. Stegmann C, Hochdorfer D, Lieber D, Subramanian N, Stohr D, Laib Sampaio K,
737 Sinzger C. 2017. A derivative of platelet-derived growth factor receptor alpha binds
738 to the trimer of human cytomegalovirus and inhibits entry into fibroblasts and
739 endothelial cells. PLoS Pathog 13:e1006273.
740 51. Powers C, Fruh K. 2008. Rhesus CMV: an emerging animal model for human CMV.
741 Med Microbiol Immunol 197:109-15.
742 52. Wang D, Li G, Schauflinger M, Nguyen CC, Hall ED, Yurochko AD, von Einem J, Kamil
743 JP. 2013. The ULb' region of the human cytomegalovirus genome confers an
744 increased requirement for the viral protein kinase UL97. J Virol 87:6359-76.
745 53. Sinzger C, Hahn G, Digel M, Katona R, Sampaio KL, Messerle M, Hengel H,
746 Koszinowski U, Brune W, Adler B. 2008. Cloning and sequencing of a highly
747 productive, endotheliotropic virus strain derived from human cytomegalovirus
748 TB40/E. J Gen Virol 89:359-68.
749 54. Li G, Rak M, Nguyen CC, Umashankar M, Goodrum FD, Kamil JP. 2014. An epistatic
750 relationship between the viral protein kinase UL97 and the UL133-UL138 latency
751 locus during the human cytomegalovirus lytic cycle. J Virol 88:6047-60.
752

753

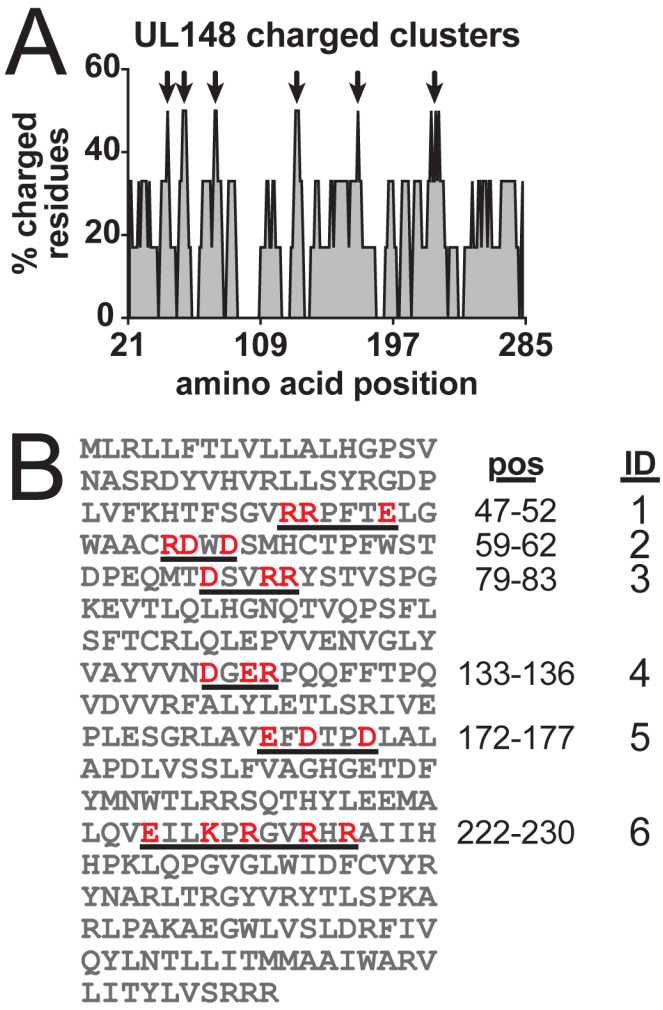

FIGURE 1. Charged amino acid clusters within the predicted UL148 ectodomain. (A) Percentage of charged residues (K, R, D, E) within the predicted UL148 ectodomain identified using an iterative scanning window six amino acid residues in size. Black arrows designate charged clusters (>40% charged residues). The last three local maxima in close proximity were treated as a single cluster. (B) UL148 protein sequence. Amino acid positions (pos) of the identified charged clusters are underlined. Residues in red were mutated to alanine in the six constructs indicated above using sequential numbering (ID), starting from the amino-terminus.

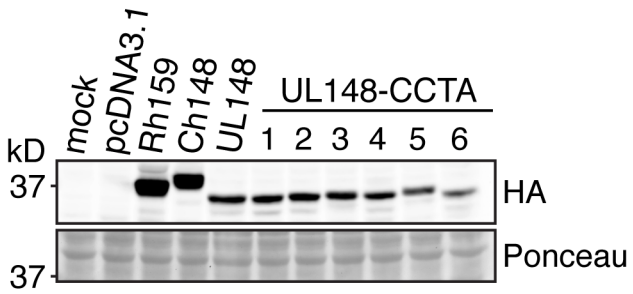

FIGURE 2. Expression of HA-tagged UL148 CCTA mutants and UL148 homologs. Human embryonic kidney 293T cells were transfected with expression plasmids encoding the indicated HA-tagged proteins. At 48 h post-transfection, cell lysates were analyzed by Western blot.

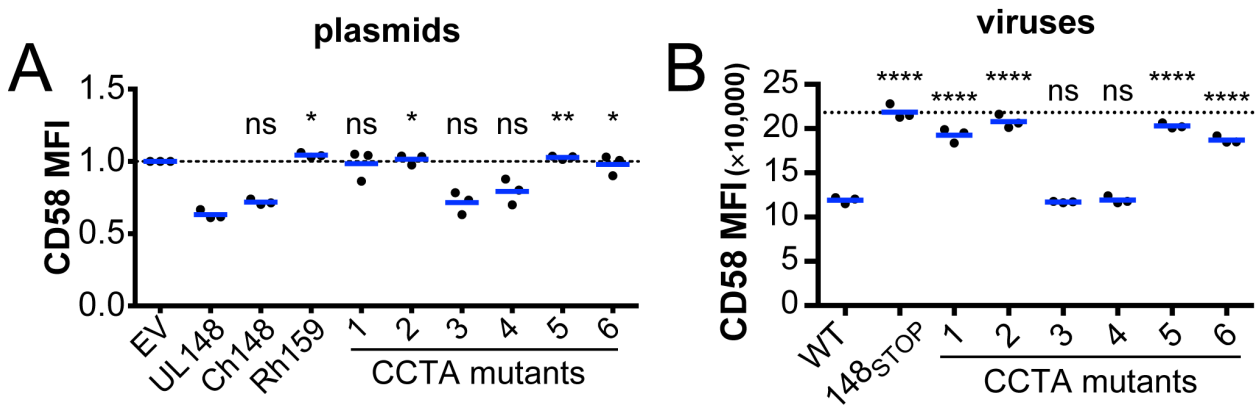

FIGURE 3. Analysis of cell surface CD58 levels during expression of UL148 CCTA mutants and homologs from other primate CMVs. (A) A549 cells were transfected with plasmids expressing the indicated protein or empty vector (EV). At 72 h post-transfection, cell surface CD58 levels were analyzed by flow cytometry. Median fluorescence intensity (MFI) values were normalized to the EV control. (B) Fibroblasts (HFFT) were infected at an MOI of 2 $TCID_{50}$ per cell with HCMV strain TB40/E derivatives wildtype for *UL148* (WT), carrying the indicated UL148 CCTA mutations, or *UL148*-null (148_{STOP}). At 72 h post-infection, cell surface CD58 was quantified by flow cytometry. (A-B) Data points indicate biological replicates from three independent experiments. P-values comparing the mean of each condition to wildtype UL148 (UL148, panel A) or wildtype virus (WT, panel B) were obtained by one-way analysis of variance (ANOVA) with Tukey's correction for multiple comparisons: ns, not significant; *, $p < 0.05$; **, $p < 0.01$; ****, $p < 0.0001$.

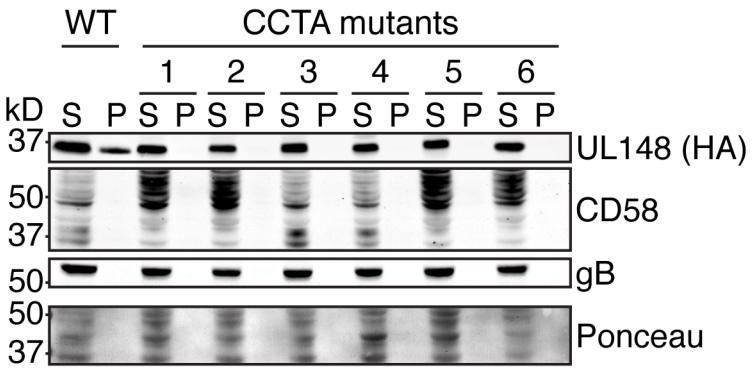

FIGURE 4. The propensity of UL148 to accumulate in a detergent-insoluble form is not required to block CD58 maturation. Fibroblasts (HFFT) were infected at an MOI of 1 $TCID_{50}$ per cell with wildtype HCMV (WT) or the indicated *UL148* mutant (CCTA mutants 1-6). At 72 h post-infection, cell lysates were separated by centrifugation into supernatant (S) containing soluble proteins and pellet (P) containing insoluble proteins. Supernatant and pellet fractions were analyzed by Western blot for UL148, CD58, and gB levels.

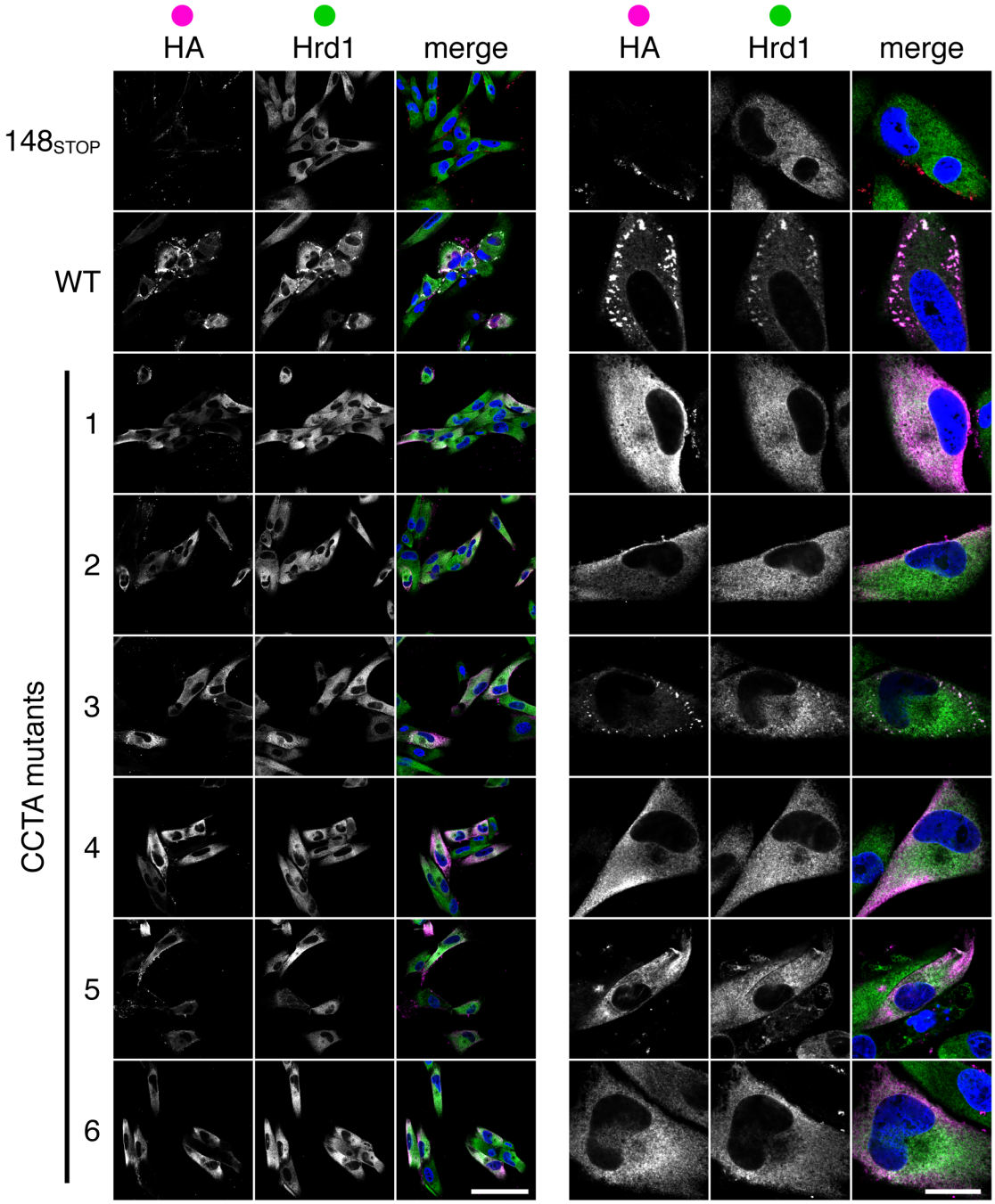

FIGURE 5. Mutation of five UL148 charged clusters abolishes punctate co-localization of UL148 and ER marker Hrd1. Fibroblasts (HFFT) were infected at an MOI of 1 $TCID_{50}$ per cell with HCMV strain TB40/E wildtype for *UL148*, harboring the indicated *UL148* CCTA mutant, or entirely null for *UL148* (148_{STOP}). At 72 h post-infection, cells were fixed and imaged by confocal microscopy after staining with antibodies specific for HA ($UL148^{HA}$, magenta) or ER marker Hrd1 (green). Nuclei were counterstained using Hoechst dye (blue).

807

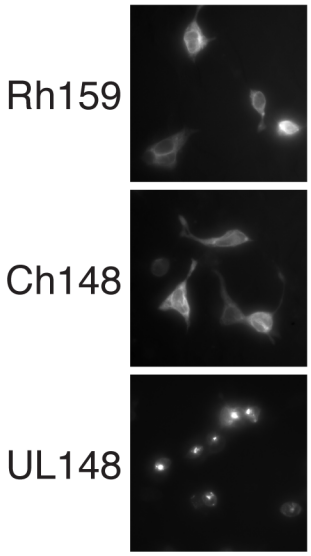

808

809 **FIGURE 6. Localization of UL148, Rh159, and Ch148.** Human embryonic kidney 293T
810 cells were transfected with doxycycline-inducible vectors encoding the indicated protein
811 fused to a GFP tag. 100 ng/mL doxycycline was added to cells 1 h post-transfection. At
812 48 h post-transfection, GFP signal was visualized by immunofluorescence microscopy.
813
814
815
816
817
818
819

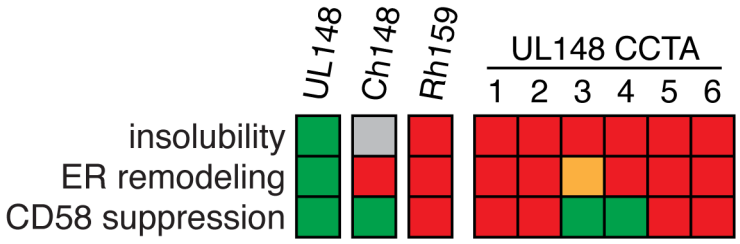

FIGURE 7. Summary of activities of CCTA mutants of UL148 and UL148 homologs. Green squares indicate activity indistinguishable from wild-type HCMV UL148. Red squares indicate total absence of the activity. Yellow squares indicate a partial phenotype. Gray square, not tested.